Kovove Mater. 48 2010 117–126
DOI: 10.4149/km_2010_2_117

A study of microstructure and solidification behaviour of Zn-Cu alloy

U. Böyük[1]*, S. Engin[2], H. Kaya[1], E. Çadırlı[3], N. Maraşlı[4], K. Keşlioğlu[4]

[1]*Department of Science Education, Education Faculty, Erciyes University, 38039 Kayseri, Turkey*
[2]*Institute of Science and Technology, Department of Physics, Erciyes University, 38039 Kayseri, Turkey*
[3]*Department of Physics, Faculty of Arts and Sciences, Niğde University, 51240 Niğde, Turkey*
[4]*Department of Physics, Faculty of Arts and Sciences, Erciyes University, 38039 Kayseri, Turkey*

Received 27 May 2009, received in revised form 1 October 2009, accepted 2 October 2009

Abstract

Zn-1.5wt.%Cu peritectic alloy was prepared in a graphite crucible under a vacuum atmosphere. Unidirectional solidification of Zn-1.5wt.%Cu peritectic alloy was carried out with the Bridgman method by using metals of 99.99 % purity under the argon atmosphere and two different conditions; with a temperature gradient (G) range of 1.99–7.81 K mm^{-1} at constant growth rate (V) and a growth rate range of 8.41–661.11 μm s^{-1} at a constant temperature gradient. The microstructures of the directionally solidified Zn-1.5wt.%Cu peritectic samples were observed to be cellular. From both transverse and longitudinal sections of the samples, cellular spacing (λ), and cell tip radius (R) were measured and expressed as functions of solidification processing parameters (G and V) using a linear regression analysis. The experimental results were also compared with values calculated according to the current theoretical and numerical models, and similar previous experimental results.

K e y w o r d s: metals & alloys, peritectic solidification, cellular growth, crystal growth

1. Introduction

Solidification and melting are transformations between crystallographic and non-crystallographic states of a metal or alloy. These transformations are of course basic to such technological applications as ingot casting, foundry casting, continuous casting, single crystal and growth directional solidification of composite alloys. An understanding of the mechanism of solidification and how it is affected by such parameters as temperature distribution, solidification conditions and alloying, is important in the control of mechanical properties of the cast metals and fusion welds [1].

Peritectic alloys occupy an outstanding position among the engineering materials. Many technically important alloy systems such as steels, Cu alloys, rare earth permanent magnets and high Tc superconductors display peritectic reactions where phase and microstructure selection plays an important role for the processing and the properties of the material [2]. Despite the practical importance of peritectic alloys, the variety of complex solidification microstructures that can form in these alloys has drawn the recent attention of researches to this field [3].

Peritectic microstructures are characterized by the growth competition between η primary and a peritectic ε phase, which can both coexist with the liquid at the peritectic temperature T_p. When peritectic alloy is directionally solidified under planar growth conditions, the rejection of solute in the liquid leads to the formation of a solute boundary layer [4]. The composition in the liquid at the interface increases as the single-phase solidification and the interface temperature decrease with time until a steady-state growth conditions are achieved at the solidus temperature of the alloy. The three phase peritectic reaction ($L + \varepsilon \rightarrow \eta$) cannot occur at T_p but must occur below T_p. However, below T_p, η can also form directly by crystallization from liquid and unless the temperature is maintained constant, all the η can be produced this way [5].

*Corresponding author: tel.: +90 352 437 4901 # 37096; fax: +90 352 437 88 34; e-mail address: boyuk@ercives.edu.tr

The Zn-Cu alloy system, which is the typical peritectic alloy with cellular structure, has recently attracted much attention. Therefore the Zn-Cu system was selected as a model system to investigate the cellular structure in peritectic alloys. Moreover, Zn-Cu alloy is an excellent alloy system to study coupled growth for three main reasons: firstly, Zn-Cu is a typical binary peritectic system in which four peritectic reactions occur over the whole composition range, secondly, in contrast to many other peritectic systems, the mushy zone range is small ($\sim 3\,\mathrm{K}$), which makes it convenient to carry out experiments, thirdly, all necessary physical parameters related to the Zn-Cu system are well known.

1.1. Theoretical models for cellular spacing

In directional solidification experiments, the solidification processing parameters, temperature gradient (G) and growth rate (V) can be independently controlled so that one may study the dependence of microstructure parameter (λ) on either G at constant V or V at constant G for the constant initial solute composition (C_o). Most experimental studies have shown that the microstructural parameters decrease as solidification processing parameters (G and V) increase, for the constant C_o. A literature survey shows several theoretical models [6–8] and numerical models [9–11] used to examine the influence of solidification processing parameters (G, V, C_o) on the microstructure parameter.

Hunt [6], Kurz and Fisher [7] and Trivedi [8] have derived cellular/dendritic spacing formulas, which apply for steady-state conditions, as a function of G, V and C_o. Hunt and Lu [9] and Kurz, Giovanola and Trivedi [10, 11] have proposed numerical models to characterize cells and primary dendrite spacing during steady-state growth conditions, as a function of V and C_o. The theoretical and numerical models for determination of cellular spacing proposed by these authors are given by Eqs. (1)–(5):

$$\lambda = 2.83\,[\Gamma m(k_\mathrm{o}-1)C_\mathrm{o}D]^{0.25}\,G^{-0.5}V^{-0.25}$$
(Hunt model [6]), (1)

$$\lambda = 4.3\left[\frac{\Gamma m(k_\mathrm{o}-1)C_\mathrm{o}D}{k_\mathrm{o}^2}\right]^{0.25} G^{-0.5}V^{-0.25}$$
(Kurz-Fisher model [7]), (2)

$$\lambda = 2.83\,[L\Gamma m(k_\mathrm{o}-1)C_\mathrm{o}D]^{0.25}\,G^{-0.5}V^{-0.25}$$
(Trivedi model [8]), (3)

$$\lambda = 4.09\,k_\mathrm{o}^{-0.745}\left[\frac{\Gamma k_\mathrm{o}}{mC_\mathrm{o}(k_\mathrm{o}-1)}\right]^{0.41} D^{0.59}V^{-0.59}$$
(Hunt-Lu model [9]), (4)

$$\lambda = 4\pi\left[\frac{\Gamma D k_\mathrm{o}}{mC_\mathrm{o}(k_\mathrm{o}-1)}\right]^{0.5} V^{-0.5}$$
(Kurz-Giovanola-Trivedi model [10, 11]), (5)

where Γ is the Gibbs-Thomson coefficient, m is the liquidus line slope, k_o is the partition coefficient, C_o is the initial alloy composition, D is the diffusion coefficient in the liquid, L is in the range of 10–28 that depends on harmonic perturbations.

1.2. Dendritic/cellular tip radius

As mentioned in the previous section, the Hunt [6], Kurz-Fisher [7] and Trivedi [8] models have been applied to find the relationships between R as a function of V and C_o. According to the Hunt model [6],

$$R = \left[\frac{2\Gamma C_\mathrm{o}D}{\mathrm{m(k_o-1)}}\right]^{0.5} V^{-0.5}, \tag{6}$$

according to the Kurz-Fisher model [7],

$$R = 2\pi\left[\frac{\Gamma C_\mathrm{o}D}{\mathrm{m(k_o-1)}}\right]^{0.5} V^{-0.5}, \tag{7}$$

and according to the Trivedi model [8],

$$R = \left[\frac{2k_\mathrm{o}\Gamma C_\mathrm{o}DL}{\mathrm{m(k_o-1)}}\right]^{0.5} V^{-0.5}. \tag{8}$$

As can be seen from Eqs. (6)–(8), the theoretical models for dendritic/cellular tip radius, R are also very similar and the difference among them is a constant only.

In this work, the theoretical models for high growth rate were chosen because the experiments were carried out for high growth rates ($V > V_\mathrm{cs}$, where V_cs is the critical velocity at which the planar interface becomes unstable), and the experimental results were compared to the results obtained by the theoretical and numerical models. Also several experimental studies in the literature [12–25] were compared with these theoretical predictions under steady-state growth conditions, for alloys of different systems: Zn-Cu [12, 13], Zn-Al [14, 15], Al-Cu [16, 17], Al-Si [18], Fe-Si [19], Fe-Cr [20], Pb-Bi [21], Ni-Al [14, 22], Zn-Ag [23], NaCl [24], and Pivalic acid-ethanol [25] and an agreement between theory and experiment is generally reported.

Thus, the purpose of the present work is to experimentally investigate the effect of solidification processing parameters on the microstructure parameters in the Zn-Cu peritectic alloy and to compare the results with the current theoretical and numerical models and similar previous experimental results.

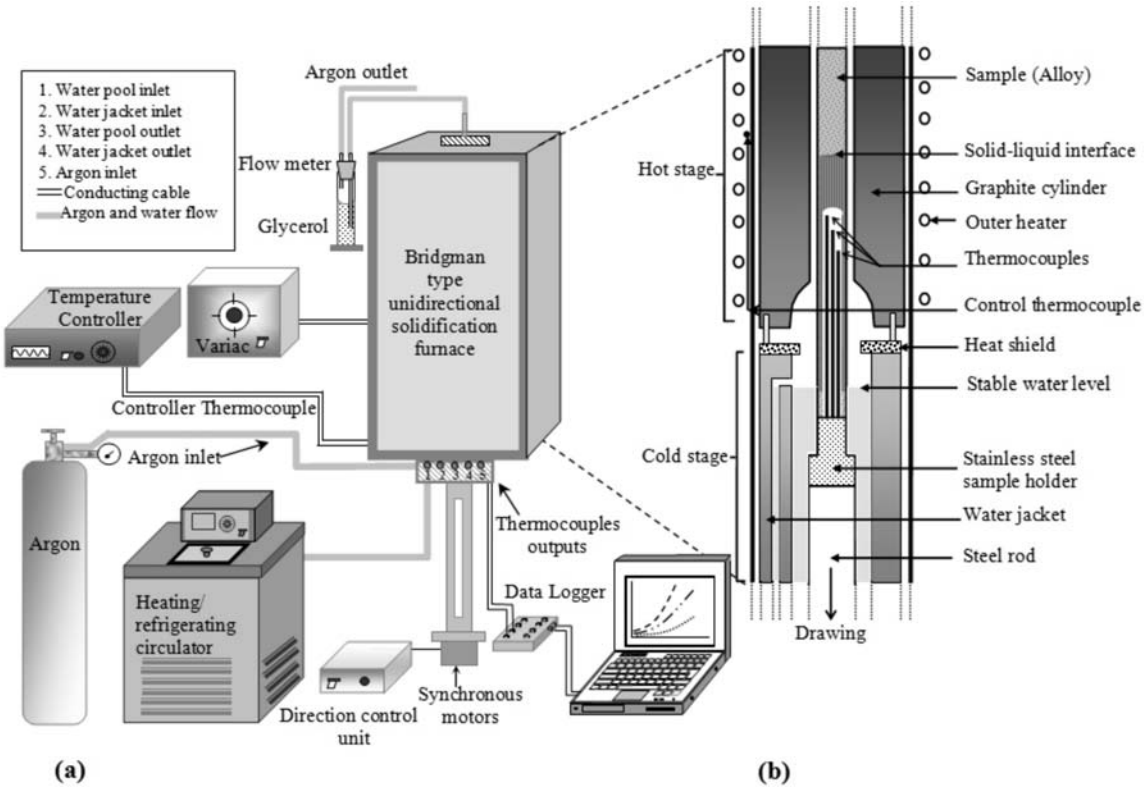

Fig. 1. (a) Block diagram of the experimental setup, (b) the details of the Bridgman type directional solidification furnace.

2. Experimental apparatus and procedure

2.1. Sample preparation and solidification

Zn-Cu peritectic alloy was prepared by using metals of 99.99 % purity. Weighed amounts of Zn and Cu metals were melted in a graphite crucible, which was placed into a vacuum-melting furnace. After allowing time for melt homogenisation, the molten alloy was poured into the prepared 13 graphite crucibles (200 mm in length 4 mm ID and 6.35 mm OD) held in a hot filling furnace. Then each specimen was positioned in a graphite cylinder (300 mm in length, 10 mm ID and 40 mm OD) in a Bridgman type furnace. After stabilizing the thermal conditions in the furnace under an argon atmosphere, the specimen was grown by pulling it downwards at various solidification conditions by means of synchronous motors. Specimens were solidified under steady state conditions with different G (1.99–7.81 K mm^{-1}) at a constant V (16.44 μm s^{-1}) and with different V (8.41–661.11 μm s^{-1}) at a constant G (7.81 K mm^{-1}). After 10–12 cm steady-state growth, the samples were quenched by rapidly pulling it down into the water reservoir. The temperature of water in the reservoir was kept at approximately 300 K to an accuracy of ±0.1 K using a *Poly Science digital 9102* model heating/refrigerating circulating bath and the temperature in the sample was controlled to an accuracy of ±0.1 K by using a *Eurotherm 2604* type controller. The block diagram of the experimental set-up and details of the Bridgman type directional solidification furnace are shown in Fig. 1.

2.2. Measurements of temperature gradient and growth rate

The temperature of the Bridgman type furnace was controlled to about ±0.1 K with a *Eurotherm 2604* type temperature controller. Throughout the experiment, temperature distribution was obtained by measuring the temperatures in the sample by three thermocouples (type-K), which were placed within the samples. The thermocouples were placed into capillary alumina tubes (0.8 mm ID, 1.2 mm OD) which were positioned approximately 10 mm apart and parallel to the heat flow direction inside the crucible. All thermocouples were connected by coaxial cables to a data-logger interfaced with a computer, and the temperature data were acquired automatically. When the second thermocouple was at the solid-liquid interface and the third thermocouple in the liquid, their temperatures were used to determine G values. The temperature gradient ($G = \Delta T/\Delta X$) for each sample was determined using the measured values of ΔT and the known value of ΔX.

The time taken for the solid-liquid interface to pass through the thermocouples separated by known dis-

Table 1. The experimental results and relationships between the cellular spacing and solidification parameters for the Zn-Cu peritectic alloy

Solidification parameters		Microstructure parameters				
G (K mm^{-1})	V (μm s^{-1})	λ_T (μm)	λ_L (μm)	λ_m (μm)	λ_M (μm)	R (μm)
1.99	16.44	232.20 ± 8.76	213.53 ± 11.0	173.04 ± 10.25	264.99 ± 12.34	70.72 ± 3.20
3.33	16.44	167.47 ± 8.39	155.52 ± 7.76	130.75 ± 6.71	200.50 ± 8.93	63.91 ± 2.64
4.64	16.44	147.31 ± 7.51	130.38 ± 8.89	116.56 ± 6.41	166.38 ± 9.17	51.94 ± 1.82
6.50	16.44	115.23 ± 6.17	103.99 ± 6.70	90.91 ± 5.18	135.48 ± 7.26	46.64 ± 1.73
7.81	16.44	106.03 ± 5.16	95.58 ± 4.51	80.53 ± 3.49	122.60 ± 5.33	41.59 ± 1.62
7.81	**8.41**	159.92 ± 5.05	99.45 ± 4.63	78.08 ± 3.59	128.94 ± 5.38	52.43 ± 1.81
7.81	**16.44**	106.03 ± 5.16	95.58 ± 4.51	80.53 ± 3.49	122.60 ± 5.33	41.59 ± 1.62
7.81	**40.42**	100.87 ± 4.52	72.25 ± 4.06	53.38 ± 3.42	89.21 ± 5.08	28.74 ± 1.74
7.81	**75.75**	77.82 ± 3.23	53.94 ± 3.07	42.07 ± 2.35	68.03 ± 3.34	19.73 ± 0.87
7.81	**165.27**	62.96 ± 1.97	45.44 ± 2.11	33.13 ± 1.77	56.05 ± 2.41	12.72 ± 0.69
7.81	**661.11**	46.99 ± 1.13	32.47 ± 1.03	22.77 ± 0.85	41.05 ± 1.22	6.34 ± 0.41

Relationships	Constant (k)	Correlation constant (r^2)
$\lambda_T = k_1 G^{-0.57}$	$k_1 = 341.97$ (μm$^{0.43}$ K$^{0.57}$)	$r_1^2 = -0.992$
$\lambda_T = k_2 V^{-0.26}$	$k_2 = 255.04$ (μm$^{1.26}$ s$^{-0.26}$)	$r_2^2 = -0.970$
$\lambda_L = k_3 G^{-0.59}$	$k_3 = 323.59$ (μm$^{0.41}$ K$^{0.59}$)	$r_3^2 = -0.996$
$\lambda_L = k_4 V^{-0.27}$	$k_4 = 189.67$ (μm$^{1.27}$ s$^{-0.27}$)	$r_4^2 = -0.978$
$\lambda_m = k_5 G^{-0.55}$	$k_5 = 123.87$ (μm$^{0.45}$ K$^{0.55}$)	$r_5^2 = -0.986$
$\lambda_m = k_6 V^{-0.30}$	$k_6 = 165.57$ (μm$^{1.30}$ s$^{-0.30}$)	$r_6^2 = -0.972$
$\lambda_M = k_7 G^{-0.56}$	$k_7 = 257.04$ (μm$^{0.44}$ K$^{0.56}$)	$r_7^2 = -0.998$
$\lambda_M = k_8 V^{-0.28}$	$k_8 = 246.61$ (μm$^{1.28}$ s$^{-0.28}$)	$r_8^2 = -0.980$
$R = k_9 G^{-0.43}$	$k_9 = 95.49$ (μm$^{0.57}$ K$^{0.43}$)	$r_9^2 = -0.988$
$R = k_{10} V^{-0.46}$	$k_{10} = 162.18$ (μm$^{1.46}$ s$^{-0.46}$)	$r_{10}^2 = -0.998$

λ_T – average values of cellular spacing measured from the transverse section of the samples by area counting and triangle methods,
λ_L – the values of the cellular spacing measured from the longitudinal section,
λ_m – the minimum values of the cellular spacing measured from the longitudinal section,
λ_M – the maximum values of the cellular spacing measured from the longitudinal section,
R – the values of the cell tip radius measured from the longitudinal section.

tances was read from the data-logger record. Thus, the value of growth rate ($V = \Delta X/\Delta t$) for each sample was determined using the measured values of Δt and ΔX. The calculated values of G and V are given in Table 1.

2.3. Metallographic analysis

The unidirectionally grown quenched samples were removed from the graphite crucible, then ground to observe the solid-liquid interface, and longitudinal (parallel to the growth direction) section, which included the quenched interface, was separated from the sample. The longitudinal and transverse sections of ground samples were then cold mounted with epoxy-resin. The longitudinal and transverse sections were ground flat with 180, 500, 1000, 2500 grit SiC papers, and polished with 6 μm, 3 μm, 1 μm, 0.25 μm and 0.05 μm diamond paste. After polishing, the samples were etched in a solution (20 g CrO_3 plus 3 g Na_2SO_4 in 100 ml distilled water) for 5 s. After metallographic preparation, the microstructures of the samples were revealed. The microstructures were characterized from both transverse and longitudinal sections of samples using an *Olympus BX-51* optical microscopy. Typical images of growth morphologies of directionally solidified Zn-1.5wt.%Cu alloy are shown in Fig. 2.

The quantitative chemical composition analysis of solid phases in the sample was carried out by a *LEO scanning electron microscopy* (SEM) equipped with an energy dispersive X-ray (EDX) spectrometer as well as a computer controlled image system. At peritectic temperature (697 K), the solid solubility of Cu in Zn and the solid solubility of Zn in Cu are 2.7 weight pct Zn and 39 weight pct Cu, respectively [26]. According to EDX results (Fig. 3) and the solid solubility of all phases, the dark phase is Cu-based solid solution (Cu-39wt.%Zn), the grey phase is η phase (Zn-2.7wt.%Cu) and the composition of the peritectic liquid is about 0.4 wt.% Cu.

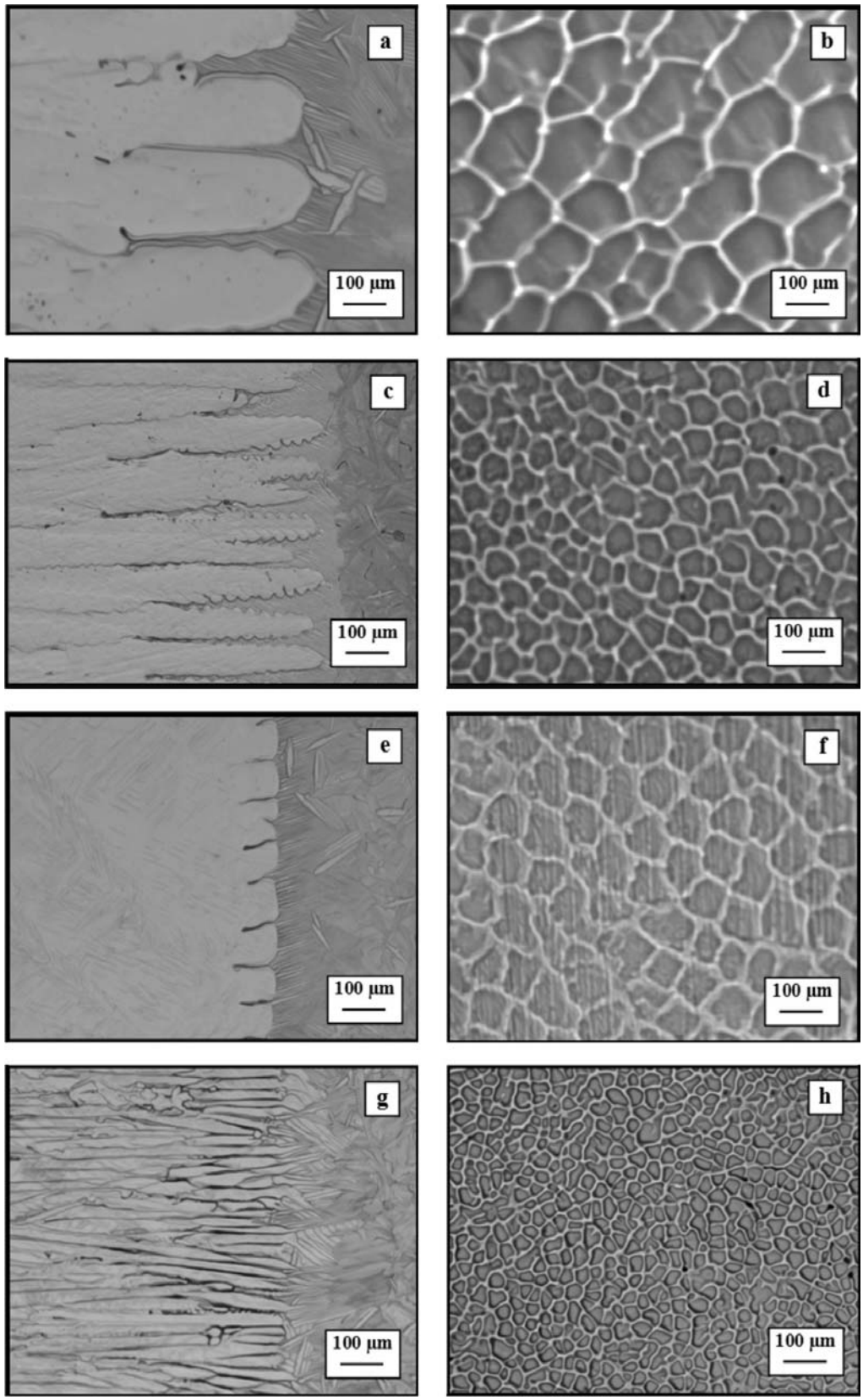

Fig. 2. Typical optical images of the growth morphologies of directionally solidified Zn-1.5wt.%Cu alloy: (a) longitudinal section, (b) transverse section ($G = 1.99\ \mathrm{K\,mm^{-1}}$, $V = 16.44\ \mu\mathrm{m\,s^{-1}}$), (c) longitudinal section, (d) transverse section ($G = 7.81\ \mathrm{K\,mm^{-1}}$, $V = 16.44\ \mu\mathrm{m\,s^{-1}}$), (e) longitudinal section, (f) transverse section ($G = 7.81\ \mathrm{K\,mm^{-1}}$, $V = 8.41\ \mu\mathrm{m\,s^{-1}}$), (g) longitudinal section, (h) transverse section ($G = 7.81\ \mathrm{K\,mm^{-1}}$, $V = 661.11\ \mu\mathrm{m\,s^{-1}}$).

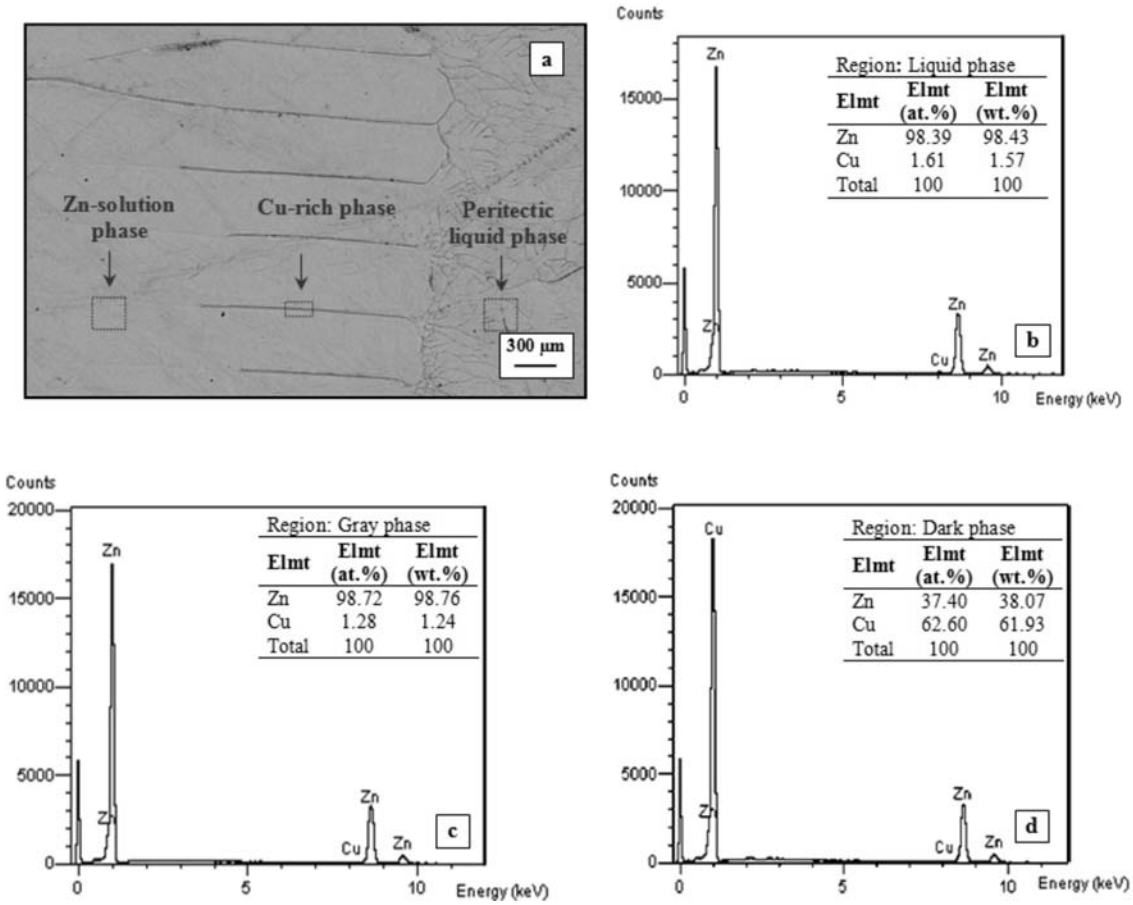

Fig. 3. (a) The chemical composition analysis of the Zn-1.5wt.%Cu alloy by using SEM and EDX, (b) quenched liquid phase, (c) grey phase (Zn-based solid solution), (d) dark phase (Cu-rich phase).

2.4. Measurements of cellular spacing and cell tip radius

The major mechanisms by which the adjustment in cellular spacing occurs are well documented in the literature [27]. The regimes of unstable primary spacing for cellular structures were determined. In this case, cellular elimination occurred when the local spacing was smaller than the stable spacing. In contrast, if the local primary spacing is larger than the stable spacing, then a new cell is created by the mechanism of tip-splitting. As in the case of the cellular structure, the unstable ranges of spacing were characterized by measuring the largest spacing, $\lambda_{\max}$, at which dendrite elimination occurred, and the smallest spacing $\lambda_{\min}$, at which tip splitting occurred.

The measurements of the cellular spacing λ_{m} (minimum), λ_{M} (maximum) and λ_{L} (average values of λ_{m} and λ_{M}), which are the distance between nearest two cell tips, were made on the longitudinal sections of the samples. As can be seen from Table 1, the relationship between the values of λ_{L}, λ_{M} and λ_{m} for the steady growth were obtained to be $\lambda_{\mathrm{m}} < \lambda_{\mathrm{L}} < \lambda_{\mathrm{M}}$.

Two different methods were used for measurement of the cellular spacing on the transverse sections. The first method is the triangle method [28]. The triangle is occurred by joining the centres of the three neighbouring cells (Fig. 4b), and sides of the triangle corresponded to $\lambda_{\mathrm{tr.}}$ The second method is the area counting method [29]. In this method, the average cellular spacing values (Fig. 4c), λ_{ar}, were calculated from

$$\lambda_{\mathrm{ar}} = \frac{B}{M}\left(\frac{A}{N}\right)^{0.5}, \tag{9}$$

where B (1.075 for hexagonal structures) is correction factor, M is the magnification factor, A ($A = a \times b$) is the total specimen cross-section area and N is the number of cell on the cross-section. The value of λ_{T} is the average of λ_{ar} and λ_{tr} given in Table 1.

The dendrite tip radius, defined in Fig. 4d, was measured by fitting a suitable circle to the cell tip side. These measurements were repeated at least 30–40 times on the cells for each G and V.

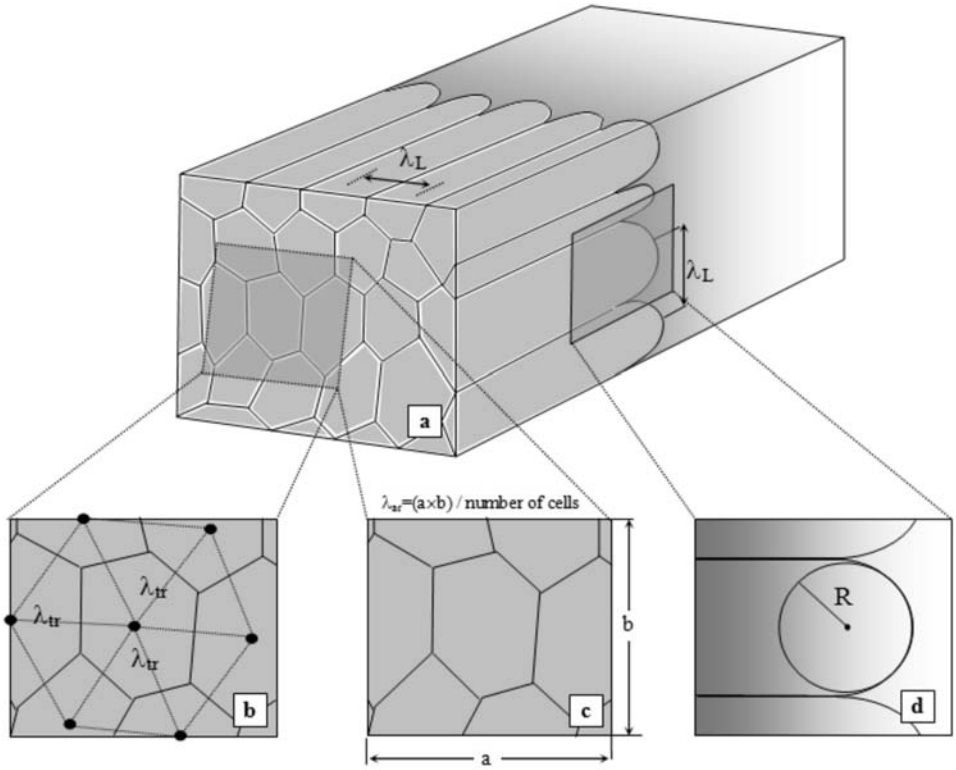

Fig. 4. Schematic illustration of the cellular spacing measurements on transverse and longitudinal sections: (a) schematic illustration of the microstructure, (b) triangle method for measuring that cellular spacing, (c) area counting method for measuring that cellular spacing, (d) schematic illustration of cell tip radius.

3. Results and discussion

3.1. Influence of the temperature gradient on the cellular spacing and cell tip radius

A series of experiments were carried out with different G (1.99–7.81 $\mathrm{K\,mm^{-1}}$) at a constant V (16.44 $\mu\mathrm{m\,s^{-1}}$) and also with different V (8.41–661.11 $\mu\mathrm{m\ s^{-1}}$) at a constant G (7.81 $\mathrm{K\,mm^{-1}}$) for the Zn-1.5wt.%Cu peritectic alloy. Figure 2 shows the views of cellular spacing from longitudinal and transverse sections of the specimen to investigate the influence of solidification processing parameters on the cellular spacing. As expected, the formation of the microstructure has varied with the temperature gradient (G) at a constant growth rate (V). As the values of G were increased, the cellular spacing λ_i (λ_T, λ_L, λ_m, λ_M) and cell tip radius (R) decreased. The highest values for λ and R were obtained at the minimum value of G (1.99 $\mathrm{K\,mm^{-1}}$), as shown in Fig. 2a and Table 1. A high temperature gradient allows more intense atomic diffusion. Thus, the highest values of λ and R are attributed to the more intense cooperative growth and to a higher diffusion length.

The variation of λ and R versus G is essentially linear on the logarithmic scale. As can be seen from Table 1 and Fig. 5a, the data form straight lines, the linear regression analysis gives the proportionality equation for constant V as:

$$\lambda_\mathrm{i} = kG^{-a}, \tag{10}$$

$$R = kG^{-b}, \tag{11}$$

where λ_i represents the values of λ_T, λ_L, λ_m, λ_M and k is a constant, a and b are exponent values relating to the temperature gradients for λ_i and R, respectively. The relationships between the cellular spacing and temperature gradient were determined by linear regression analysis and are given in Table 1. As can be seen from Fig. 5a and Table 1, the exponent values relating to the temperature gradient (G) for λ_T, λ_L, λ_m and λ_M were found to be –0.57, –0.59, –0.55, and –0.56, respectively. The exponent value relating to the temperature gradient (G) for R was found to be –0.43.

The influence of temperature gradient (G) on the cellular spacing λ and dendrite tip radius R cannot be ignored. The influence of temperature gradient on the values of G and R was investigated by several authors [18, 19] for different binary alloys. The exponents relating to the temperature gradient (G) for λ obtained in the present work are in a good agreement with the

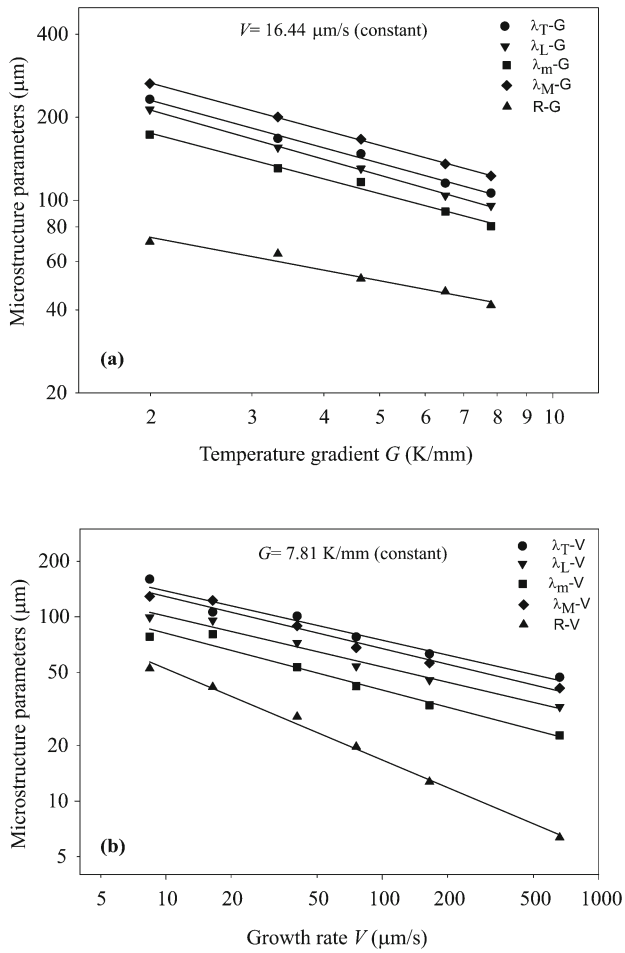

Fig. 5. (a) Variation of λ as a function of G at a constant V (16.44 μm s^{-1}), (b) variation of λ as a function of V at a constant G (7.81 K mm^{-1}) for Zn-1.5wt.%Cu alloy.

exponent values relating to the temperature gradient (G) for λ obtained in the range from –0.45 to –0.60 by various researchers [18–25] for different alloy systems.

Table 1 and Fig. 5b show variations of λ_i (λ_T, λ_L, λ_m, λ_M) and R with V at the constant G (7.81 K mm^{-1}) for the Zn-1.5wt.%Cu alloy. The variation of λ versus the growth rate was plotted on the logarithmic scales and it is essentially linear. A linear regression analysis gives the proportionality equations between the growth rate (V) and solidification parameters (λ and R) as

$$\lambda_i = kV^{-c}, \tag{12}$$

$$R = kV^{-d}, \tag{13}$$

where c and d are exponent values relating to the growth rate for λ_i and R. Figure 5b shows clearly that an increase in V produces a decrease in λ_i and R. The exponent values relating to the growth rate for λ_T, λ_L, λ_m and λ_M were found to be –0.26, –0.27, –0.30, and –0.28, respectively. The exponent value relating to the growth rate for R was found to be 0.46. The exponent values of V (–0.26, –0.27, –0.30, and –0.28) obtained in this work are in good agreement with the range exponent values of V (from –0.24 to –0.33) obtained by various researchers [18–25] for different alloy systems. And also, the exponent value of R for Zn-1.5wt.%Cu alloy obtained in the present work is mostly in a good agreement with the exponent values of R obtained in previous work [20–25] for different alloy systems.

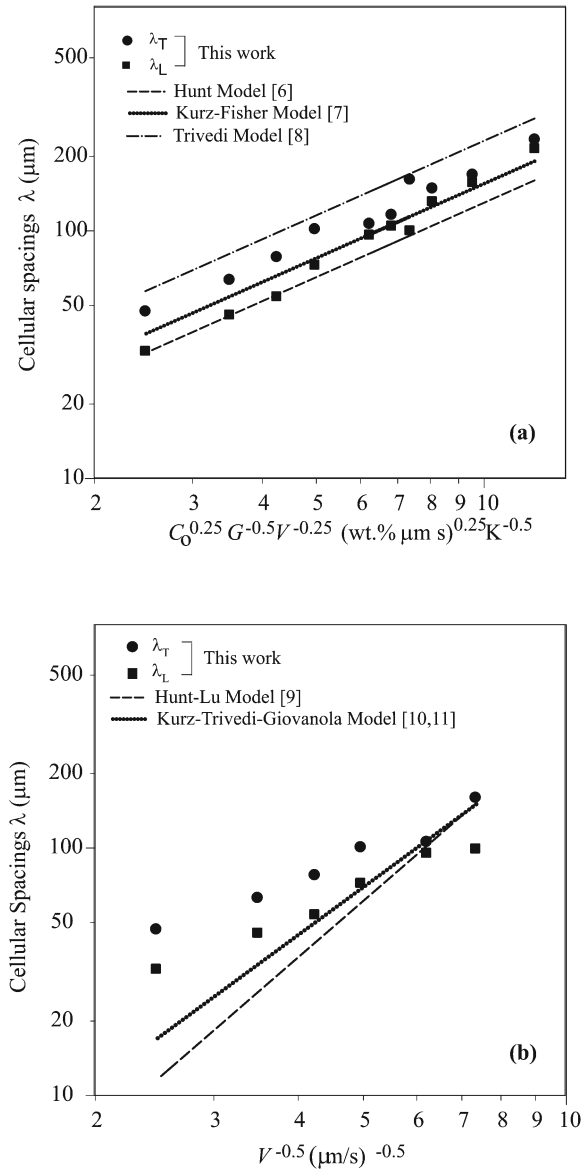

Fig. 6. (a) Comparison of cellular spacing, λ, obtained in the present experimental work with predicted values of λ by the theoretical models [6–8] for Zn-1.5wt.%Cu alloy, (b) comparison of cellular spacing, λ, obtained in the present experimental work with predicted values of λ by the numerical models [9–11] for Zn-1.5wt.%Cu alloy.

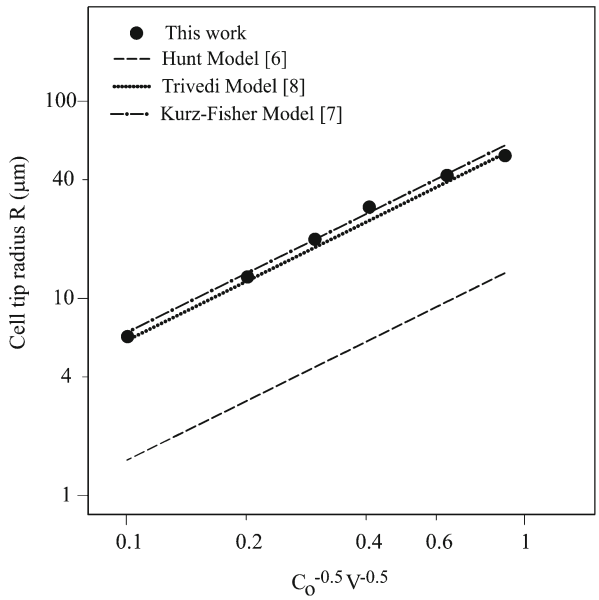

Fig. 7. Comparison of cell tip radius, R, obtained in the present experimental work with predicted values of R by the theoretical models [6–8] for Zn-1.5wt.%Cu alloy.

3.2. Comparison of the experimental results with theoretical models

The comparison of the experimentally obtained λ and R values in the present work with the λ and R values calculated by the Hunt [6], Kurz-Fisher [7], Trivedi [8], Hunt-Lu [9] and the Kurz-Giovanola-Trivedi [10, 11] models are given in Figs. 6 and 7. The thermophysical parameters of the Zn-1.5wt.%Cu alloy [30, 31] used in the λ and R calculations of the theoretical models are given in Appendix A. As can be seen from Fig. 6a, the calculated values of λ using Hunt [6] and Kurz-Fisher [7] models are in a good agreement with the experimental λ_T and λ_L values, but the calculated values of λ with the Trivedi [8] model give slightly higher values than the experimental ones.

The comparison of our experimental values of λ with the calculated values of λ by the Hunt-Lu [9] and Kurz-Giovanola-Trivedi [10, 11] numerical models is given in Fig. 6b. As can be seen in Fig. 6b, our experimental results generally do not agree with the calculated values of λ by the Hunt-Lu [9] and Kurz--Giovanola-Trivedi [10, 11] models. This might be due to the fact that the theoretically exponent values of V according to the Hunt-Lu [9] and Kurz-Giovanola--Trivedi [10, 11] numerical models are (–0.59 and –0.50, respectively) are about twice that of our experimentally determined exponent value of V (–0.26).

Figure 7 shows the comparison of the experimentally obtained R values as a function of $(C_o V)^{-0.5}$ at a constant G with the values of R calculated by the Hunt [6], Kurz-Fisher [7] and Trivedi [8] models. It can be seen from Fig. 7, the calculated values of R by Kurz-Fisher [7] and Trivedi [8] models are in a good agreement with our experimental values. The calculated values of R by the Hunt [6] model are much smaller than our experimental values.

4. Summary and conclusions

The principal results of the present work can be summarized as follows:

1. The values of microstructure parameters (λ_T, λ_L, λ_m, λ_M and R) decrease as the values of G and V increase. The exponent values relating to the temperature gradient (from –0.55 to –0.59) for cellular spacing agree well with the previous experimental results.

2. The experimental λ values are very close to those predicted by the Hunt [6] and Kurz-Fisher [7] models but are higher than the values predicted by the Trivedi model [8] and are higher than our experimental λ values. On the other hand, the experimental λ values disagree with the values obtained by Hunt-Lu [9] and Kurz-Giovanola-Trivedi [10, 11] numerical models.

3. The values of R measured in the present work are in a good agreement with the calculated values according to Hunt [6], Kurz-Fisher [7] and Trivedi [8] models.

Acknowledgements

This research was financially supported by the The Scientific and Technical Research Council of Turkey (TÜBİTAK under Contract No: 107T095). The authors are grateful to TÜBİTAK for their financial support.

References

[1] PORTER, D. A.—EASTERLING, K. E.: Phase Transformations in Metals and Alloys. Second Edition. Cheltenham, UK, CRC Press 1992, p. 185.
[2] HUNZIKER, O.—VANDYOUSSEFI, M.—KURZ, W.: Acta Mater., *46*, 1998, p. 6325. doi:10.1016/S1359-6454(98)00336-X
[3] KERR, H.W.—KURZ, W.: Inter. Mater. Rev., *41*, 1996, p. 29.
[4] TRIVEDI, R.—PARK, J. S.: J. Cryst. Growth, *235*, 2002, p. 572. doi:10.1016/S0022-0248(01)01803-6
[5] ST JOHN, D. H.: Acta Metall., *38*, 1990, p. 631. doi:10.1016/0956-7151(90)90218-6
[6] HUNT, J. D.: Solidification of Casting of Metals. London, Metals Society 1979.
[7] KURZ, W.—FISHER, D. J.: Acta Metall., *29*, 1981, p. 11. doi:10.1016/0001-6160(81)90082-1
[8] TRIVEDI, R.: Metall. Trans., 15A, 1984, p. 977.
[9] HUNT, J. D.—LU, S. Z.: Metall.Trans., *27A*, 1996, p. 611.
[10] KURZ, W.—GIVANOLA, B.—TRIVEDI, R.: Acta Metall., *34*, 1986, p. 823. doi:10.1016/0001-6160(86)90056-8

[11] KURZ, W.—GIVANOLA, B.—TRIVEDI, R.: J. Cryst. Growth, *91*, 1988, p. 123. doi:10.1016/0022-0248(88)90376-4
[12] LI, Y.—NG, S. C.—MA, D.—JONES, H.: Scripta Metall., *39*, 1998, p. 7. doi:10.1016/S1359-6462(98)00112-2
[13] MA, D.—LI, Y.—NG, S. C.—JONES, H.: Sci. Technol. Adv. Mat., *2*, 2001, p. 127. doi:10.1016/S1468-6996(01)00038-9
[14] COOKSEY, D. J.—MONSON, D.—WILKINSON, M. P.—HELLAWELL, A.: Met. Trans. Soc. AIME, *218*, 1964, p. 745.
[15] TUNCA, H.—SMITH, R. W.: J. Mater. Sci., *23*, 1988, p. 111. doi:10.1007/BF01174041
[16] YOUNG, K. P.—KIRKWOOD, D. H.: Metal. Mat. Trans., *6A*, 1975, p. 197.
[17] SHARP, R. M.—HELLAWELL, A.: J. Cryst. Growth, *6*, 1970, p. 253. doi:10.1016/0022-0248(70)90076-X
[18] PRATT, R. A.—GRUGEL, R. N.: Mater. Charac., *31*, 1993, p. 225. doi:10.1016/1044-5803(93)90066-5
[19] ALBERNY, R.—SERRA, J.—TURPIN, M.: Trans. Met. Soc. AIME, *245*, 1969, p. 55.
[20] LEE, J. H.—KIM, H. C.—JO, C. Y.—KIM, S. K.—SHIN, J. H.—LIU, S.—TRIVEDI, R.: Mat. Sci. Eng. A, *413–414*, 2005, p. 306. doi:10.1016/j.msea.2005.09.021
[21] TOKIEDA, K.—YASUDA, H.—OHNAKA, I.: Mat. Sci. Eng. A, *262*, 1999, p. 238. doi:10.1016/S0921-5093(98)01005-3
[22] LEE, J.—VERHOEVEN, J. D.: J. Cryst. Growth, *144*, 1994, p. 353. doi:10.1016/0022-0248(94)90477-4
[23] XU, W.—FENG, Y. P.—LI, Y.—ZANG, G. D.—LI, Z. Y.: Acta Materalia, *50*, 2002, p. 83.
[24] GORBUNOV, A. V.: Acta Metall., *40*, 1992, p. 513.
[25] TRIVEDI, R.—MASON, J. T.: Metal. Mat. Trans. A, *22*, 1991, p. 235.
[26] CHOU, K.—ZHOU, G.—CHEN, W.: Fundamentals of Structural Chemistry. Singapore, World Scientific Publishing Co. 1993.
[27] WALKER, D. J.—MULLIS, A. M.: J. Mat. Sci., *36*, 2001, p. 865. doi:10.1023/A:1004882614044
[28] GANESAN, S.—CHAN, C. L.—POIRIER, D. R.: Mater. Sci. Eng. A, *151*, 1992, p. 97. doi:10.1016/0921-5093(92)90186-5
[29] BHAT, M. S.—POIRIER, D. R.—HEINRICH, J. C.: Metall. Trans. B, *26*, 1995, p. 1049. doi:10.1007/BF02654107
[30] MASSALSKI, T. B.: Binary Alloy Phase Diagrams. Materials Park, OH, American Society for Metals 1986.
[31] LIU, H. Y.—JONES, H.: Acta Metall., *40*, 1992, p. 229. doi:10.1016/0956-7151(92)90298-S

Appendix A

Thermophysical parameters of Zn-Cu peritectic alloy

Property	Symbol	Unit	Value	References
Melting point of Zn	T_m	K	692.73	[30]
Melting point of Cu	T_m	K	1358.02	[30]
Liquidus temperature Zn-Cu alloy	T_L	K	699.37	[30]
Peritectic temperature of Zn-Cu alloy	T_P	K	696.58	[30]
Composition	C_o	wt.%	1.5	[30]
Slope of liquid line	m_L	K wt.%$^{-1}$	3.19	[30]
Gibbs-Thomson coefficient	Γ	µm K	0.11	[31]
Diffusion coefficient (liq.)	D_L	µm^2 s^{-1}	2040	[31]
Distribution coefficient	k	–	1.62	[31]
The harmonic perturbations	L	mJ m^{-2}	10	[8]